SCEC Report: 2018 SCEC Proposal: Monitoring Seasonally-Driven Stress Changes on Faults within the Plate Boundary Zone in California using cGPS Observations

Using horizontal cGPS (Plate Boundary Observatory, PBO) observations of crustal displacements processed by University of Nevada Reno's (UNR) Geodetic Laboratory and NSF's GAGE Facility at UNAVCO, we quantify non-steady-state horizontal deformation fields within the plate boundary zone in California for the last thirteen years, leading up to the 2019 Magnitude (Mw) 7.1 Ridgecrest Earthquake. We use the geodetic network processing tool of Holt and Shcherbenko (2013) and Kraner et al. (2018). We also determine the associated Coulomb stress changes on existing fault structures through time. Our results show that the time-dependent strain anomalies are associated with seasonal variations as well as longer-term changes such as drought and anomalously heavy precipitation. To investigate the physics behind the non-steady-state deformation patterns, we compare our results with two different hydrologic loading models.

Our compilation of the thirteen-year transient strain history in Southern California highlights a remarkable long-wavelength pattern of seasonal anomalies that impact the horizontal strains in parts of Northern, Central, and Southern California by as much as ± 10-20 x 10^{-9} and Coulomb stress changes on faults by ± 1 kPa (Figure 1). During most summers a seasonal positive dilatational strain anomaly develops along the San Andreas Fault (SAF) zone between 34° N – 37.5° N (Figure 1b). The Great Valley and the Sierra Nevada move up to 2 mm toward the Great Basin with respect to the Pacific plate reference during the summer, resulting in positive Coulomb stress changes on the SAF. During the winter, on the other hand, the horizontal displacement patterns reverse and dilatational compressions are observed along the SAF (Figure 1a). Opposite to the patterns on the San Andreas, the right-lateral strike-slip faults in the Eastern California Shear Zone (ECSZ), east of the Sierra Nevada and north of the Garlock Fault, undergo extensional dilatation during the winter (Figure 1a), and vice versa (Figure 1b).

The magnitude of the seasonal patterns appear to vary during the severe drought between 2012 and 2015 and the heavy precipitation years of 2017 and 2019. Our model detects significantly diminished signals during the drought (Figure 1c, d) and augmented signals during the wet years (Figure 1e, f) compared to normal years. We hypothesize that these seasonal and longer-term variations in the long-wavelength horizontal deformation mostly occur due to the variations in the surface water loads from the precipitation patterns in California (e.g Argus et al., 2014 and Borsa et al., 2014). In order to test the hypothesis, we investigate and compare our long-wavelength model with two different hydrologic models. The first model is UNAVCO hydrologic displacement model derived from Noah 0.125˚grid Land Surface Model for North American Land Data Assimilation System (NLDAS) (Puskas et al., 2017). The hydrologic model displacements are calculated with Green's functions for each PBO station within the grid (Farrell, 1972; Wahr et al., 2013). This model is GPS-independent, generated using three parameters in the surface model as inputs (soil moisture, snow load, and total canopy water storage). We also took Argus et al.'s (2017) surface water estimates (inferred from vertical cGPS) and computed the same Green's function elastic response in the horizontal field (Kim et al., 2018) using JPL's modeling software ISSM-SESAW v1.0 (Adhikari et al., 2016). We analyze these two hydrologic predictions using the same algorithm used to analyze the actual horizontal cGPS data to quantify the history of hydrologic-loading-related deformation in California (Figure 2). We then calculate the Root Mean Square Error (RMS) and correlations between the three predicted dilatational strain fields as a function of corresponding misfit to GPS (Standard Error of Unit Weight – SEUW) to compare the

models quantitatively (Figure 3). The Size of SEUW varies with damping level in the inversion; higher damping yields higher SEUW and longer wavelength strain anomalies. Lower damping tends to match the higher amplitude anomalies. The comparisons show that long wavelength models (higher damping) yield spatiotemporal similarities to the hydrologic loading models, especially for areas north of latitude 35º, including for the drought and heavy precipitation patterns. However, significant differences between the hydrologic loading models and the model inferred from cGPS appear in the regions south of latitude 34º N after the spring of 2010. We infer the reason for these differences is most likely from the post-seismic relaxation from the 2010 El Mayor-Cucapah Earthquake in Baja California. The average correlation coefficients between the models are 0.56 (with the UNAVCO hydrologic model), and 0.44 (with the loading estimates provided by Argus et al., 2017) (Figure 3a).

In our previous results we show that just prior to the 2014 Mw 6.0 South Napa Earthquake of August 24, there was a Coulomb stress increase of 5.1 ± 1.6 kPa on right-lateral faults in the region of the event, caused by a seasonal positive dilatational strain anomaly there (Kraner et al., 2018). We examined non-tectonic stress changes in South Napa from 2007–2014 and find non-tectonic positive Coulomb stress changes in each summer (Figure 4a). With a similar damping level used to analyze Napa region, we investigate the Ridgecrest region (Figure 5). We find that a positive Coulomb stress change of ~1kPa develops on faults every May and June between 2008 and 2019 in the region (Figure 4b, red). The long-wavelength transient strain/stress model (which matches the hydrologic loading models) can only explain up to ~15% of the Coulomb stress increases observed every May –June in the Ridgecrest region (Figure 4b, blue). The source of these positive Coulomb stress anomalies needs to be investigated further. The difficulty is that the regional coverage for this wavelength of anomaly is spatially aliased by GPS station spacing. In the case of Napa, Interferometric Synthetic Aperture Radar (InSAR) provided improved spatial resolution and magnitude of seasonal strain anomalies (Kraner et al., 2018).

Our next goal is to detect other regions that experience such periodic seasonal stress changes and our shorter-wavelength transient strain model for the entire southern California warrants further investigation. To investigate possible dynamic sources for the shorter-wavelength strain/stress changes is more challenging owing to the spatial aliasing of the PBO network. Analyzing InSAR data may shed light on the dynamics of the shorter-wavelength variations such as groundwater-pumping (e.g. Kraner et al. 2018).

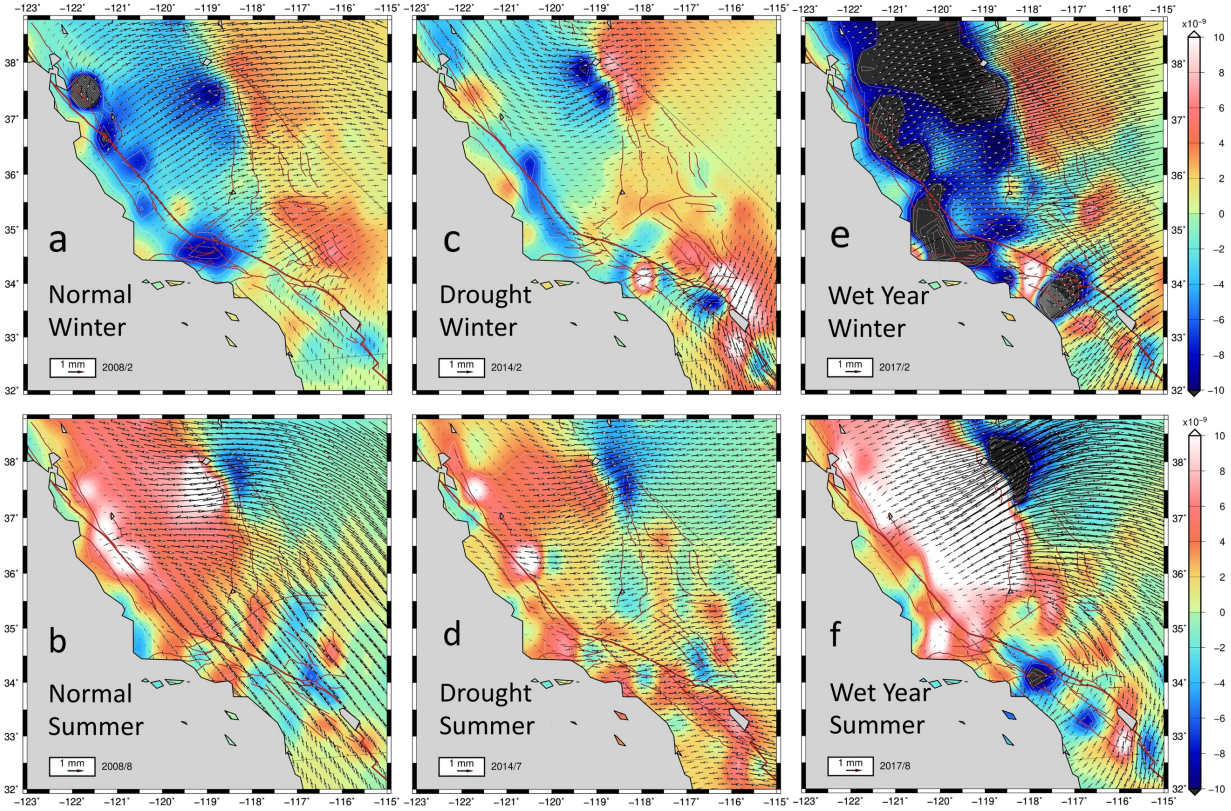

Figure 1. Model displacements relative to Pacific frame obtained from smoothed fit to seasonal components of cGPS data, with dilatational strains plotted in background for winter (a) and summer (b) of 2008. We regard this year as a normal year. The model displacements representing the drought year deformation patterns are shown in (c) for winter and (d) for the summer of 2014. Note the weak winter pattern (c) in comparison with a relatively normal winter of 2008 (a). Anomaly patterns for the drought period corresponding with the summer of 2014 (d). The deformation patterns during the heavy precipitation year of 2017 are presented for winter (e) and summer (f). The positive dilatation is extensional.

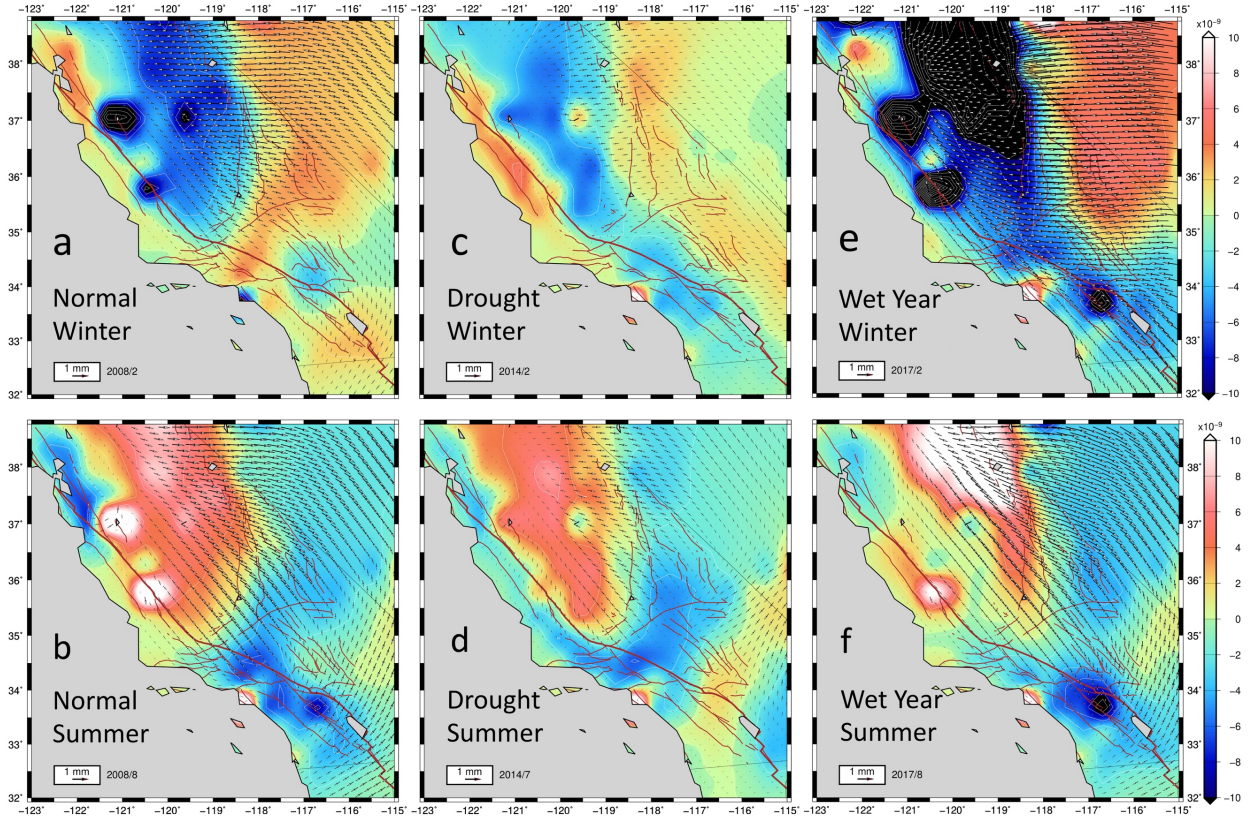

Figure 2. Model displacements relative to Pacific frame obtained from surface water equivalent estimates (Argus et al., 2017), with dilatational strains plotted in background for the normal winter (a) and summer (b) of 2008. The drought patterns are presented in (c) for the winter and (d) for the summer of 2014. Note the weak winter (c) and summer patterns (d) in comparison with the relatively larger signals for the normal winter (a) and summer (b) of 2008. The deformation patterns and motions during the heavy precipitation year of 2017 are shown in (e) for winter and (f) for summer. The positive dilatation (red) is extensional. Note that the magnitude of the scale bar is the same as in Figures 2 and 4; therefore, direct comparisons can be made between the seasonal patterns and the long-term variations.

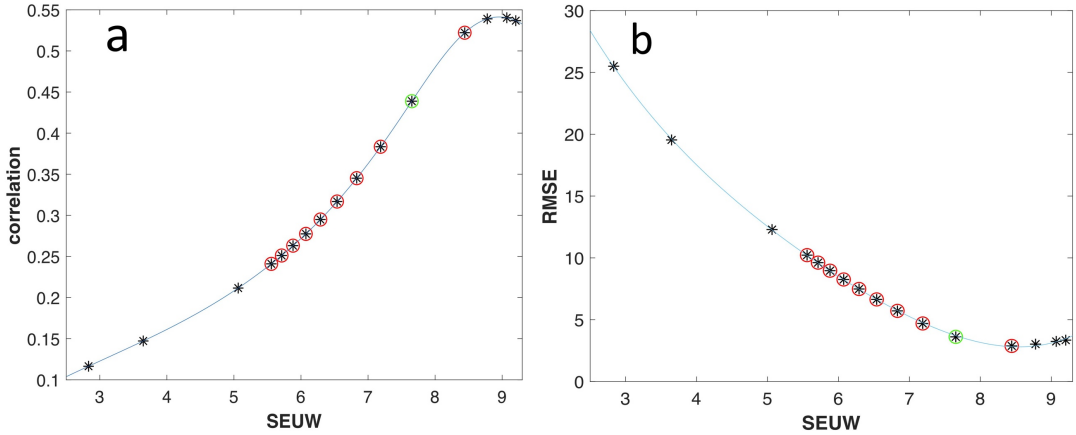

Figure 3. Statistic tests for the comparisons between the models from cGPS and the hydrologic loading estimates (Argus et al. 2017) as a function of damping levels for the horizontal long-wavelength solution. A posteriori standard error of unit weight (SEUW) is the square root of the reduced χ^2 statistic between the long-wavelength model displacement field and the GPS observations (Beavan and Haines, 2001, see A.6.). The long-wavelength solution has larger SEUW values than shorter-wavelength solutions. Values for RMSE vs. SEUW and correlation vs. SEUW result from different damping levels in the inversion of cGPS. The green circled asterisks represent the SEUW that is obtained for our chosen damping level, which provides the results in Figures 1 and 2.

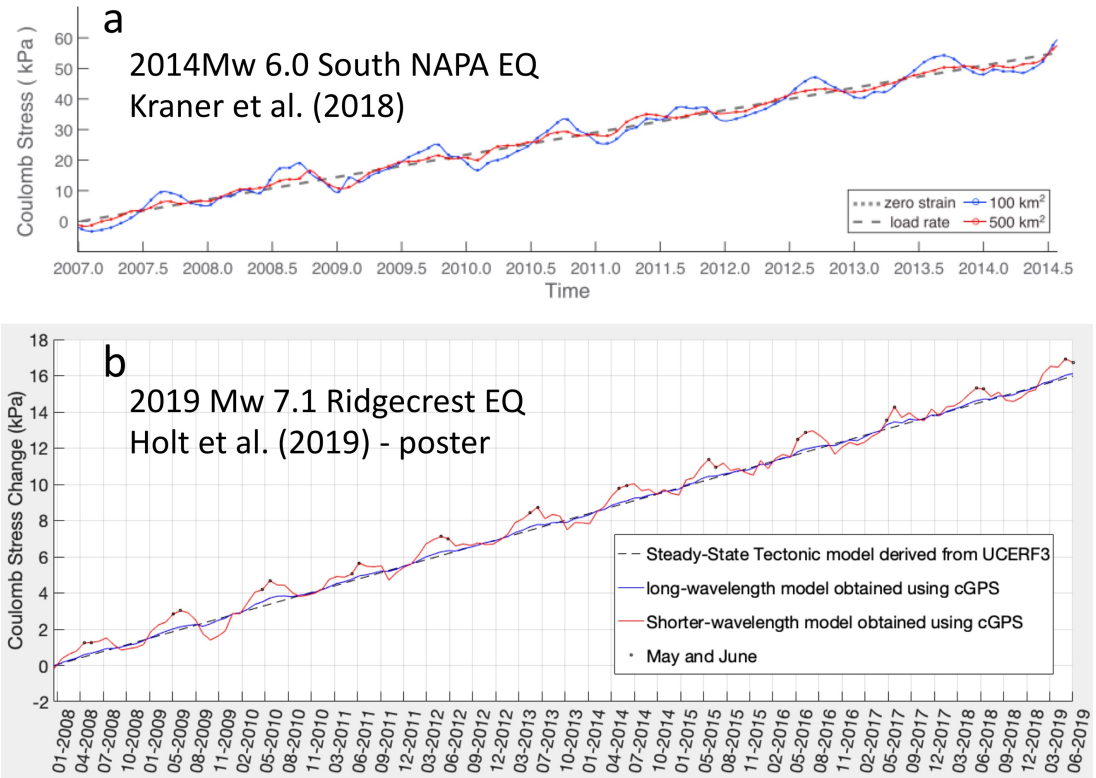

Figure 4. Time evolution of total Coulomb stress change for **(a)** South Napa region from Kraner et al. (2018) and **(b)** Ridgecrest region calculated using the same method in Kraner et al. (2018). In Ridgecrest region, seasonal Coulomb stress changes of $\pm$ 1kPa are superimposed on the steady-state tectonic stress rate ~1.4 kPa/year. We observe a positive Coulomb stress change in the region every year during the May-June period (dots).

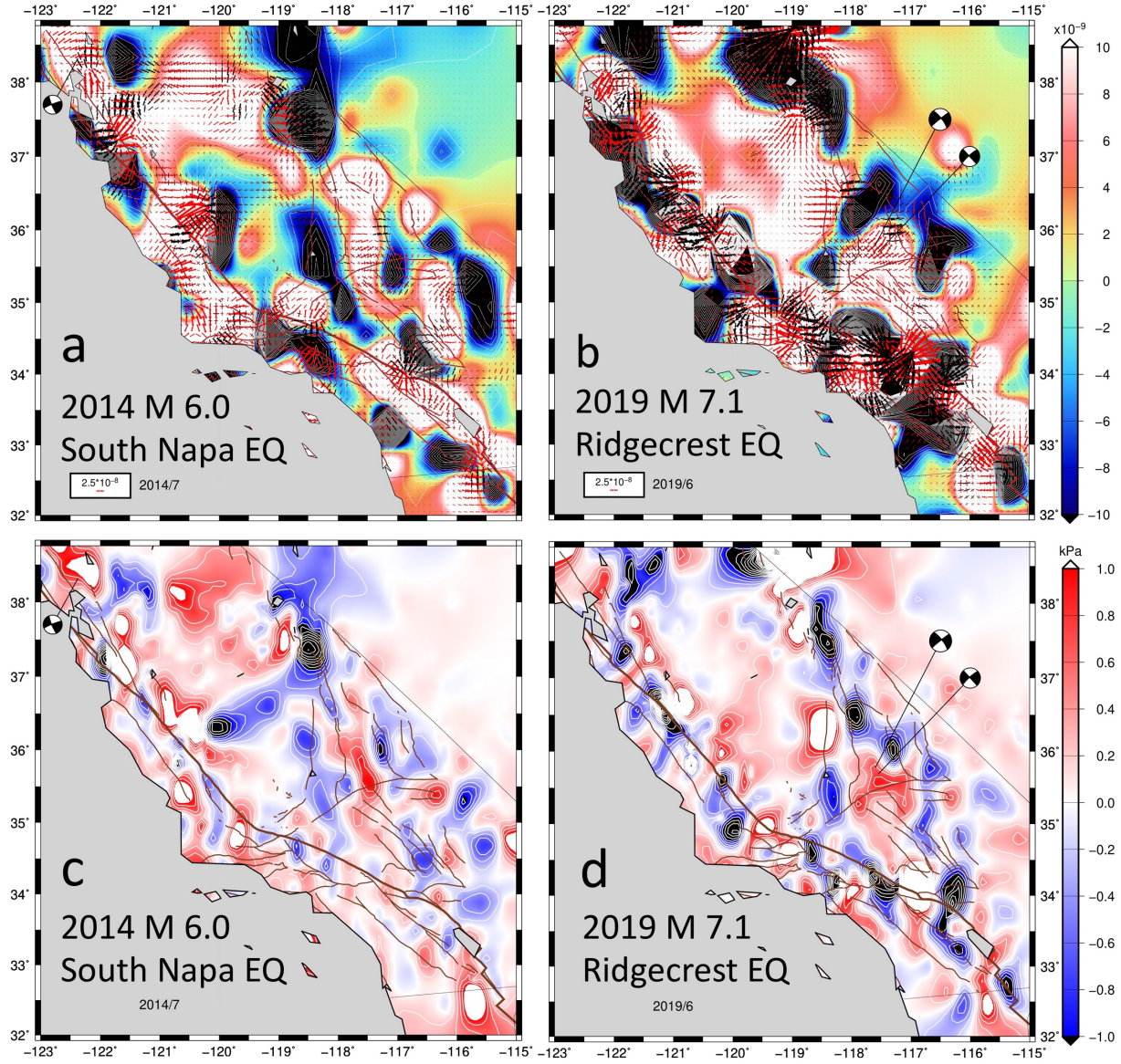

Figure 5. Seasonal anomalies: shorter-wavelength model strain field **(a, b)** and the associated Coulomb stress change **(c, d)** inferred from horizontal cGPS data for a month before the Mw 6.0 South Napa event **(a)** and **(c)** and a month before the Mw 7.1 Ridgecrest event **(b)** and **(d)**. The hotter colors indicate dilation and positive Coulomb stress changes.

References

Adhikari, S., Ivins, E. R., & Larour, E. (2016). ISSM-SESAW v1.0: mesh-based computation of gravitationally consistent sea-level and geodetic signatures caused by cryosphere and climate driven mass change. *Geoscientific Model Development*, *9*(3).

Argus, D. F., Fu, Y., & Landerer, F. W. (2014). Seasonal variation in total water storage in California inferred from GPS observations of vertical land motion. *Geophysical Research Letters*, *41*(6), 1971-1980.

Argus, D. F., Landerer, F. W., Wiese, D. N., Martens, H. R., Fu, Y., Famiglietti, J. S., ... & Watkins, M. M. (2017). Sustained water loss in California's mountain ranges during severe drought from 2012 to 2015 inferred from GPS. *Journal of Geophysical Research: Solid Earth*, *122*(12), 10-559.

Beavan, J., & Haines, J. (2001). Contemporary horizontal velocity and strain rate fields of the Pacific- Australian plate boundary zone through New Zealand. *Journal of Geophysical Research: Solid Earth*, *106*(B1), 741-770.

Blewitt, G., W. C. Hammond, and C. Kreemer (2018), Harnessing the GPS data explosion for interdisciplinary science, *Eos, 99,*https://doi.org/10.1029/2018EO104623.

Borsa, A. A., Agnew, D. C., & Cayan, D. R. (2014). Ongoing drought-induced uplift in the western United States. *Science*, *345*(6204), 1587-1590.

Farrell, W. E. (1972). Deformation of the Earth by surface loads. *Reviews of Geophysics*, *10*(3), 761-797.

Holt, W. E., Kim, J., & Bahadori, A. (2019, 11). Seasonal strain and stress changes across the western U.S. constrained using space-geodetic observations. Poster Presentation at 2019 NASA Solid Earth Team Meeting.

Holt, W. E., & Shcherbenko, G. (2013). Toward a continuous monitoring of the horizontal displacement gradient tensor field in Southern California using cGPS observations from Plate Boundary Observatory (PBO). *Seismological Research Letters*, *84*(3), 455-467.

Kim, J., Bahadori, A., & Holt, W. E. (2018,12). An eleven year history of seasonally-driven stress changes on faults within the plate boundary zone in California inferred from cGPS data. Poster Presentation at 2018 AGU Fall Meeting.

Kim, J., Bahadori, A., & Holt, W. E. (2018,08). Monitoring Seasonally-Driven Stress Changes on Faults within the Plate Boundary Zone in California using cGPS Observations. Poster Presentation at 2018 SCEC Annual Meeting.

Kraner, M. L., Holt, W. E., & Borsa, A. A. (2018). Seasonal nontectonic loading inferred from cGPS as a potential trigger for the M6. 0 South Napa earthquake. *Journal of Geophysical Research: Solid Earth*, *123*(6), 5300-5322.

Puskas, M.C., Meertens, M.C., & David, P. (2017). Hydrologic Loading Model Displacements from the National and Global Data Assimilation Systems (NLDAS and GLDAS). [online] Available at: http://www.unavco.org/data/gps-gnss/associated-products/hydrological/displacement-model-readme.pdf

Wahr, J., Khan, S. A., van Dam, T., Liu, L., van Angelen, J. H., van den Broeke, M. R., & Meertens, C. M. (2013). The use of GPS horizontals for loading studies, with applications to northern California and southeast Greenland. *Journal of Geophysical Research: Solid Earth*, *118*(4), 1795-1806.